Report

Cell Reports

Iron Toxicity in the Retina Requires *Alu* RNA and the NLRP3 Inflammasome

Graphical Abstract

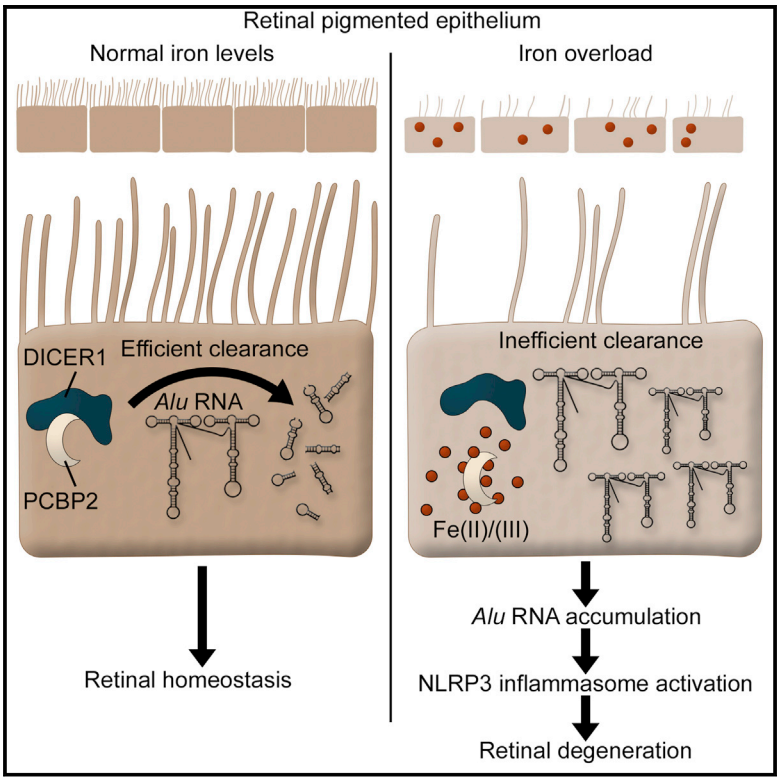

Highlights

- Iron overload induces retinal pigmented epithelium death via NLRP3 inflammasome
- SINE RNAs are intermediates of iron-induced inflammasome activation and cell death
- Iron promotes SINE RNA accumulation by inhibiting DICER1 activity
- Efficient DICER1 processing of SINE RNAs by PCBP2 is inhibited by iron overload

Authors

Bradley D. Gelfand, Charles B. Wright, Younghee Kim, ..., Philippe Georgel, Joshua L. Dunaief, Jayakrishna Ambati

Correspondence

brad.gelfand@uky.edu

In Brief

Iron overload, implicated in numerous diseases, including age-related macular degeneration, induces retinal cell death via the NLRP3 inflammasome. Gelfand et al. show that iron-induced inflammasome activation depends upon accumulation of non-coding SINE RNAs (*Alu* and B2 RNAs), which accrete due to impaired DICER1 processing.

Gelfand et al., 2015, Cell Reports *11*, 1686–1693
June 23, 2015 ©2015 The Authors
http://dx.doi.org/10.1016/j.celrep.2015.05.023

OPEN ACCESS
CellPress

Cell Reports
Report

Iron Toxicity in the Retina Requires *Alu* RNA and the NLRP3 Inflammasome

Bradley D. Gelfand,[1,2,3,*] Charles B. Wright,[1] Younghee Kim,[1] Tetsuhiro Yasuma,[1] Reo Yasuma,[1] Shengjian Li,[1] Benjamin J. Fowler,[1,4] Ana Bastos-Carvalho,[1] Nagaraj Kerur,[1] Annette Uittenbogaard,[1] Youn Seon Han,[1] Dingyuan Lou,[1] Mark E. Kleinman,[1] W. Hayes McDonald,[5] Gabriel Núñez,[6] Philippe Georgel,[7] Joshua L. Dunaief,[8] and Jayakrishna Ambati[1,4]

[1]Department of Ophthalmology and Visual Sciences
[2]Department of Biomedical Engineering
[3]Department of Microbiology, Immunology, and Human Genetics
[4]Department of Physiology
University of Kentucky, Lexington, KY 40536, USA
[5]Proteomics Laboratory, Mass Spectrometry Research Center and Department of Biochemistry, Vanderbilt University School of Medicine, Nashville, TN 37205, USA
[6]Department of Pathology and Comprehensive Cancer Center, University of Michigan Medical School, Ann Arbor, MI 48109, USA
[7]INSERM UMR_S 1109, Fédération de Médecine Translationnelle (FMTS), Université de Strasbourg, Strasbourg 67085, France
[8]F.M. Kirby Center for Molecular Ophthalmology, Scheie Eye Institute, Perelman School of Medicine, University of Pennsylvania, Philadelphia, PA 19104, USA
*Correspondence: brad.gelfand@uky.edu
http://dx.doi.org/10.1016/j.celrep.2015.05.023

SUMMARY

Excess iron induces tissue damage and is implicated in age-related macular degeneration (AMD). Iron toxicity is widely attributed to hydroxyl radical formation through Fenton's reaction. We report that excess iron, but not other Fenton catalytic metals, induces activation of the NLRP3 inflammasome, a pathway also implicated in AMD. Additionally, iron-induced degeneration of the retinal pigmented epithelium (RPE) is suppressed in mice lacking inflammasome components caspase-1/11 or Nlrp3 or by inhibition of caspase-1. Iron overload increases abundance of RNAs transcribed from short interspersed nuclear elements (SINEs): *Alu* RNAs and the rodent equivalent B1 and B2 RNAs, which are inflammasome agonists. Targeting *Alu* or B2 RNA prevents iron-induced inflammasome activation and RPE degeneration. Iron-induced SINE RNA accumulation is due to suppression of DICER1 via sequestration of the co-factor poly(C)-binding protein 2 (PCBP2). These findings reveal an unexpected mechanism of iron toxicity, with implications for AMD and neurodegenerative diseases associated with excess iron.

INTRODUCTION

Iron is a critical component of dozens of enzymatic processes and, in excess, can induce oxidative damage via Fenton's reaction, in which iron catalyzes the formation of highly reactive hydroxyl radicals. Accordingly, iron overload is implicated in the pathogenesis of numerous diseases including neurodegenerative disorders such as Alzheimer's disease, Parkinson's disease, and amyotrophic lateral sclerosis (Urrutia et al., 2014). Retinal iron overload is also implicated in the pathogenesis of age-related macular degeneration (AMD). For example, human eyes with AMD display increased iron deposition in the retina and aqueous humor (Flinn et al., 2014; Hahn et al., 2003; Jünemann et al., 2013) and animal models of iron overload reproduce AMD-like phenotypes of the retinal pigmented epithelium (RPE) and outer retina (Flinn et al., 2014; Gnana-Prakasam et al., 2012; Hadziahmetovic et al., 2008; Hahn et al., 2004). Although the damaging effects of iron overload are often attributed to oxidative damage, the precise mechanisms driving iron-induced retinal toxicity have not been defined.

Here, we report a mechanism of iron-induced retinal degeneration unique among several Fenton-capable metals that requires the specific activation of the NLRP3 inflammasome, an innate immune signaling complex recently implicated in AMD pathogenesis. We also report that iron induces NLRP3 inflammasome signaling via induction of *Alu* RNAs derived from short interspersed nuclear elements (SINEs), which are endogenous inflammasome activators abundant in human AMD. These findings suggest that the intrinsic toxicity of excess iron in the retina depends upon the activation of SINE RNA-mediated innate immune signaling.

RESULTS

Iron Overload Activates the NLRP3 Inflammasome

Given the apparent role of iron overload in retinal degeneration, we sought to determine the effect of iron on the RPE cell layer, which provides essential support to photoreceptors and the

degeneration of which demarcates atrophic AMD. The NLRP3 inflammasome is an immune signaling complex implicated in the pathogenesis of AMD (Anderson et al., 2013; Kauppinen et al., 2012; Liu et al., 2013; Marneros, 2013; Tarallo et al., 2012; Tseng et al., 2013). In models of atrophic AMD, NLRP3 inflammasome activation induces cellular death via the inflammasome effector caspase-1 (Tarallo et al., 2012). Therefore, we sought to determine whether iron overload activated the NLRP3 inflammasome. We examined mice doubly deficient in genes encoding the cellular iron exporters ceruloplasmin and hephaestin ($Cp^{-/-}Heph^{-/-}$) that exhibit age-dependent retinal iron deposition and AMD-like pathologies (Hadziahmetovic et al., 2008; Hahn et al., 2004). Similar to previous reports of human geographic atrophy tissues (Tarallo et al., 2012; Tseng et al., 2013), we detected robust expression of the inflammasome-related gene Nlrp3 in the RPE layer of $Cp^{-/-}Heph^{-/-}$ mice compared to age-matched wild-type controls (Figure 1A). We sought to determine whether acute administration of Fe(III) induced RPE degeneration and inflammasome activation. Seven days after subretinal injection of Fe(III), we detected degeneration of the RPE (Figure 1B) reminiscent of both human atrophic AMD and mouse models of NLRP3 inflammasome-induced RPE degeneration (Fowler et al., 2014; Kaneko et al., 2011; Tarallo et al., 2012). Both subretinal delivery of iron in wild-type mice and iron loading of human RPE cells induced caspase-1 maturation (Figures 1C and 1D). To further investigate the anatomic location of inflammasome activation, we assessed in situ caspase-1 activity in unfixed retinal cryo-sections by administering a caspase-1 peptide substrate that becomes fluorescent upon cleavage. We observed elevated caspase-1 proteolytic activity in the RPE cell layer of wild-type mice following iron subretinal injection (Figure S1A). We confirmed the signal was not due to accumulation of auto-fluorescent material in iron-treated wild-type mice without substrate and in iron-treated caspase-1/11 knockout mice (Figure S1B). Together, these results implicate iron overload as an inflammasome agonist in the RPE. We next sought to determine whether iron-induced inflammasome activation was due to Fenton catalytic activity. Other multivalent metal ions such as Cr(VI), Cu(I), and Zn(I) are also efficient Fenton catalysts. Loading RPE cells with metal ions induced free radical formation (Figure S1C). However, unlike Fe(III), loading human RPE cells with Cr(VI), Cu(I), or Zn(I) did not induce caspase-1 maturation (Figure S1D). These findings indicate that overload of Fenton catalytic metals alone is not sufficient to drive inflammasome activation.

Inflammasome Is Required for Iron Overload Toxicity

We next sought to determine whether inflammasome signaling contributed to iron-induced RPE degeneration. Mice lacking the inflammasome components caspase-1/11 or Nlrp3 were protected from RPE degeneration upon administration of iron compared to wild-type mice (Figures 1E and 1F). Interestingly, Nlrp3 ablation reduced RPE degeneration due to a high dose of iron injection, albeit less effectively than caspase-1/11 deficiency, implying that in response to large doses of iron, compensatory Nlrp3-independent pathways that also require caspase-1/11 contribute to RPE degeneration. Additionally, blockade of caspase-1 activity via delivery of a cell-permeable peptide inhibitor prevented RPE degeneration due to Fe(III) administration in wild-type mice (Figure 1G). Together, these data implicate the NLRP3 inflammasome in mediating iron-induced retinal toxicity.

We next tested whether other metal ions capable of participating in Fenton's reaction induced retinal toxicity. As with Fe(III), each of Cr(VI), Cu(I), and Zn(I) were toxic to the RPE cell layer (Figure 1H). However, unlike Fe(III), the toxicity of Cr(VI), Cu(I), and Zn(I) overload persisted in caspase-1/11-deficient mice (Figure 1I), suggesting that iron toxicity in this system is uniquely inflammasome dependent.

Iron Overload Causes Accumulation of *Alu*, B1, and B2 SINE RNAs

RNAs transcribed from ubiquitous *Alu* repetitive elements are inflammasome activators implicated in atrophic AMD (Dridi et al., 2012; Kaneko et al., 2011; Tarallo et al., 2012). We sought to determine whether iron overload induced *Alu* RNA accumulation. Iron overload induced elevated *Alu* RNA levels in human RPE cells (Figure 2A). Rodents also carry SINE repeats such as B1 and B2 elements that, like *Alu* repeats, are derived from non-LTR, non-autonomous retrotransposons (Jurka et al., 2005). B1 and B2 RNAs can also induce inflammasome signaling and retinal degeneration (Kaneko et al., 2011; Tarallo et al., 2012). Subretinal delivery of iron induced a dose-dependent increase in B1 and B2 RNA levels in the RPE/choroid of wild-type mice but left *Dicer1* mRNA levels unchanged (Figure 2B). Fluorescent in situ hybridization of B1 and B2 RNAs in retina of 6-month-old $Cp^{-/-}Heph^{-/-}$ mice revealed robust enrichment of these RNAs in multiple retinal layers including the RPE, choroid, and neural retina of double knockout mice compared to age-matched wild-type controls (Figure 2C).

We hypothesized that iron toxicity could be due to its ability to induce *Alu* RNAs. Administration of an *Alu* RNA-targeted antisense oligonucleotide in iron-treated human RPE cells abolished caspase-1 maturation (Figure 2D), implicating *Alu* RNA as an intermediate in this process. We previously developed an antisense oligonucleotide targeted against B2 RNA that is chemically modified for in vivo cell entry and that prevents RPE degeneration due to SINE RNA accumulation in mice (Kaneko et al., 2011; Tarallo et al., 2012). Antagonizing B2 RNA in wild-type mice prevented iron-induced RPE degeneration in four of six eyes treated with B2 antisense (compared to zero of six eyes treated with a scrambled antisense; Fisher's exact test; $p < 0.03$; Figure 2E). Collectively, these data support the concept that iron overload induces *Alu* RNA accretion and resulting inflammasome-mediated retinal toxicity.

Iron Overload Enhances DICER1-Dependent *Alu* RNA Stability

Alu RNA levels are controlled in part by the RNase DICER1 (Hu et al., 2012; Kaneko et al., 2011; Ren et al., 2012, 2013; Tarallo et al., 2012; Yan et al., 2013). We previously reported that DICER1-mediated *Alu* RNA clearance is essential for maintaining retinal health (Kerur et al., 2013; Tarallo et al., 2012). We confirmed that, as with *Alu* RNAs, both B1 and B2 RNAs are substrates for DICER1 enzymatic cleavage (Figure S2). Because free iron generates reactive oxygen species and the abundance of

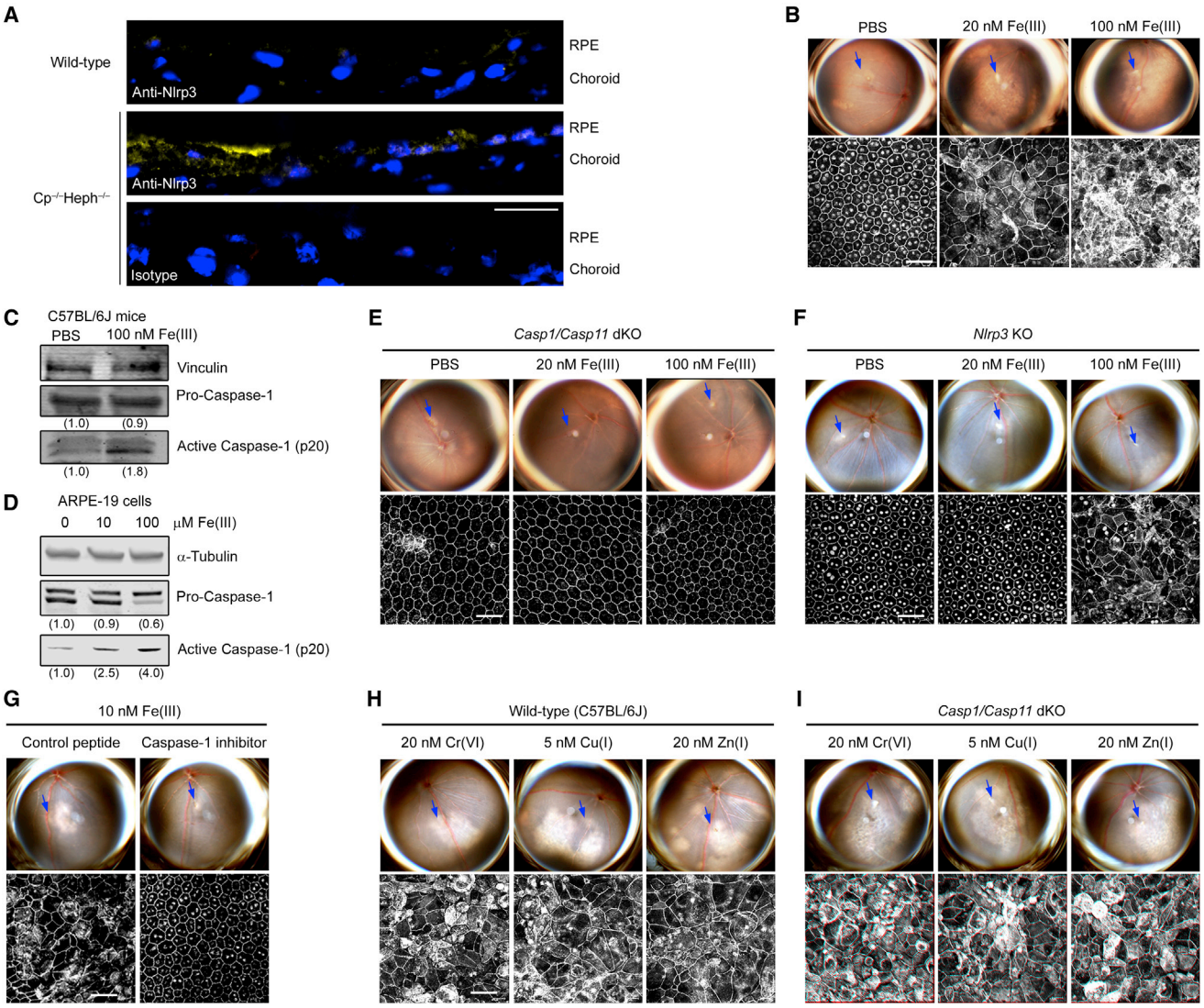

Figure 1. Iron Toxicity Depends on the NLRP3 Inflammasome

(A) Immuno-labeling of Nlrp3 (yellow signal) and nuclei (DAPI, blue signal) in the RPE/choroid of 6-month-old wild-type (top) or $Cp^{-/-}Heph^{-/-}$ mice (middle). Bottom row depicts the same area from a serial section of $Cp^{-/-}Heph^{-/-}$ immunolabeled with isotype goat IgG. Representative of n = 3 mice. The scale bar denotes 20 μm.

(B) Fundus (top) and ZO-1 staining of RPE flat mount preparations (bottom) of wild-type mice 7 days after injection of 1 μl Fe(III) at indicated concentrations. Blue arrows denote injection site.

(C and D) Western blotting of pro- and active forms of caspase-1 in ARPE-19 cells and wild-type mouse retina and RPE/choroid (pooled from four eyes) treated with indicated doses of Fe(III).

(E and F) Fundus and ZO-1 staining of RPE flat-mount preparations following delivery of Fe(III) into the subretinal space of mice lacking inflammasome components caspase-1/11 (E) and Nlrp3 (F).

(G) Fundus and ZO-1 staining of RPE flat-mount preparations of wild-type mice that received caspase-1 peptide inhibitor preceding delivery of Fe(III) into the subretinal space.

(H and I) Fundus and ZO-1 staining of RPE flat-mount preparations following administration of Cr(VI), Cu(I), or Zn(I) into the subretinal space of wild-type mice (H) and in mice lacking inflammasome components caspase-1/11 (I). Indicated doses represent the minimum concentration of metals required to consistently induce RPE degeneration.

(B–I) The scale bars denote 50 μm. Fundus images are representative of at least four replicates.

DICER1 is reduced by oxidative stress (Kaneko et al., 2011; Mori et al., 2012; Wiesen and Tomasi, 2009), we predicted that iron-induced *Alu* RNA accumulation was due to transcriptional repression of DICER1 levels. Surprisingly, iron overload did not affect DICER1 levels in RPE cells or in wild-type mice (Figures 2A and 2B). *Dicer1* mRNA was also unchanged in the RPE of 6-month-old $Cp^{-/-}Heph^{-/-}$ compared to age-matched wild-type mice (Kaneko et al., 2011), suggesting that induction of

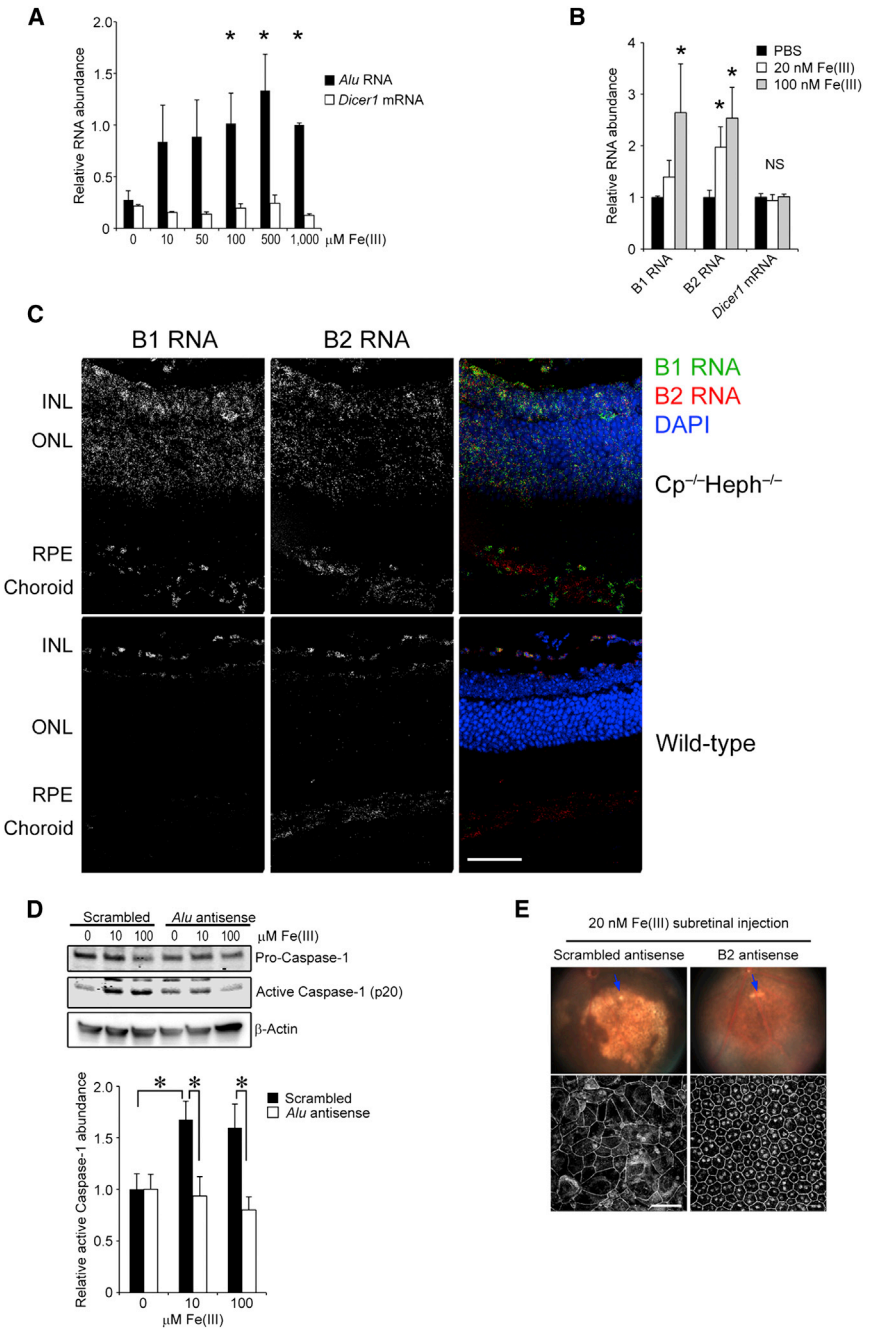

Figure 2. Iron Toxicity Depends on SINE RNA Induction

(A) Densitometry of *Alu* RNA northern blotting and real-time qPCR of *DICER1* mRNA in human ARPE-19 cells exposed to iron overload for 4 days at indicated doses.

(B) Densitometry of B1 and B2 RNAs northern blotting and real-time qPCR of *Dicer1* mRNA RPE/choroid lysates from wild-type C57BL6/J mice 7 days after subretinal injection with iron.

(C) Fluorescent in situ hybridization of B1 and B2 RNAs in retinal cross-sections of 6-month-old $Cp^{-/-}Heph^{-/-}$ (top row) or wild-type mice (bottom row). The scale bar denotes 50 μm.

(D) Western blotting of pro- and active forms of caspase-1 in ARPE-19 cells exposed to Fe(III) after treatment with either scrambled or *Alu* RNA-targeted antisense oligonucleotides.

(E) Representative fundus photographs and ZO-1-immunostained RPE flat mounts of wild-type mice treated with a cell-permeable antisense oligonucleotide targeting B2 RNA (and scrambled control) 1 day prior to subretinal injection of 10 nM Fe(III). Images were acquired 6 days after Fe(III) administration. Blue arrows denote injection site. The scale bar denotes 50 μm.

For all panels, n = 3–6; *p < 0.05. Error bars denote SEM.

Alu or B1 and B2 RNAs by iron overload was not due to suppression of DICER1 abundance.

We next sought to determine whether iron affected the stability of *Alu* RNA transcripts. Iron overload delayed RPE cell processing of a transfected biotin-labeled *Alu* RNA (Figure 3A). Further, whereas excess iron did not affect the transcription rate of endogenous *Alu* RNAs, degradation of native *Alu* RNAs was delayed as assessed by a run-on assay (Figure 3B). To determine whether iron-overload-induced *Alu* RNA accumulation involved DICER1 enzymatic activity, we examined this activity in cells treated with an antisense oligonucleotide targeting DICER1 that itself induces *Alu* RNA accumulation (Kaneko et al., 2011; Tarallo et al., 2012). In DICER1 antisense-treated cells, iron overload did not further enhance *Alu* RNA levels (Figure 3C), suggesting iron may work by suppressing DICER1 enzymatic activity. Conversely, iron did not affect recombinant human DICER1-mediated *Alu* RNA processing in vitro (Figure 3D), implicating an indirect, iron-sensitive mediator of DICER1 activity.

PCBP2 Binds to and Enhances DICER1 Processing of *Alu* RNA

We investigated potential iron-sensitive *Alu* RNA-binding partners by performing 2D liquid chromatography tandem mass spectrometry on proteins from primary human RPE cell lysates captured by pull-down of synthetic biotin-labeled *Alu* RNA. We identified poly(C)-binding protein 2 (PCBP2) (Figure S3A), an RNA-binding protein reported to be both iron sensitive and capable of modulating DICER1 enzymatic activity for micro-RNA processing (Li et al., 2012). It is reported that free cellular iron impairs DICER1 microRNA processing by decreasing its affinity for PCBP2 (Li et al., 2012). Because, like microRNAs, *Alu* RNAs are enzymatic targets of DICER1, we investigated whether a similar mechanism was responsible for iron-induced *Alu* RNA accumulation. We confirmed the interaction of PCBP2 and *Alu*

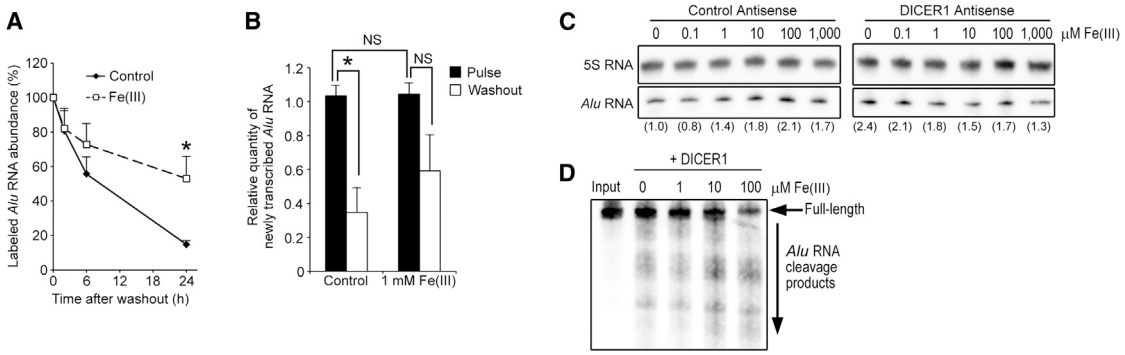

Figure 3. Iron Overload Enhances Stability of *Alu* RNA

(A) Processing of a synthetic biotin-labeled *Alu* RNA transiently transfected in ARPE-19 exposed to 1 mM Fe(III). x axis denotes time following 2-hr RNA-loading period.

(B) Quantity of endogenous *Alu* RNA accumulated during a 4-hr modified nucleotide doping pulse (4 hr) or after washout (20 hr) in ARPE-19 cells exposed to 1 mM Fe(III). *Alu* RNAs were quantified by qPCR of size-separated RNA samples, in which RNAs 100–800 nt were isolated after PAGE.

(C) Northern blotting of *Alu* RNA of human ARPE-19 cells treated with control or DICER1-targeted antisense oligonucleotides and exposed to indicated doses of Fe(III).

(D) Polyacrylamide gel separated *Alu* RNA after incubation with recombinant DICER1 in the presence of indicated quantities of Fe(III).

For all panels, n = 3–6; *p < 0.05. Error bars denote SEM.

RNA by streptavidin-mediated pull-down of a biotin-labeled *Alu* RNA followed by immunoblotting for PCBP2 (Figure 4A) and conversely via antibody-mediated pull-down of endogenous PCBP2 followed by northern blotting for native *Alu* RNA (Figure 4B). Whereas iron treatment neither impaired *Alu* RNA-DICER1 binding nor decreased PCBP2 expression, PCBP2-*Alu* RNA binding was decreased by iron overload (Figures 4A and 4B). The affinity of DICER1 for *Alu* RNA was unchanged by iron overload (Figure 4A), as is the case for DICER1 pre-microRNA processing activity inhibition by iron (Li et al., 2012). *Alu* RNA/PCBP2 binding specificity was further confirmed by performing a competition assay with 5-fold excess of unlabeled in vitro transcribed human pre-Let-7a microRNA, which binds to PCBP2 and DICER1 (Li et al., 2012) or unlabeled tRNA (with no known binding affinity for PCBP2; Figure S3B). To examine the effect of PCBP2 on DICER1-mediated processing of *Alu* RNAs, we measured the efficiency of *Alu* RNA processing by DICER1 in vitro in the presence of recombinant human PCBP2 and iron. Whereas iron or PCBP2 alone did not affect DICER1-mediated *Alu* RNA processing, recombinant PCBP2 enhanced DICER1-mediated *Alu* RNA cleavage, which was significantly impaired in the presence of iron (Figure 4C). Collectively, these data identify PCBP2 as an iron-sensitive co-factor for DICER1-mediated *Alu* RNA enzymatic processing.

DISCUSSION

Our data establish an alternative paradigm for iron-overload-induced retinal toxicity—namely that iron overload enhances *Alu* RNA stability and thereby promotes RPE degeneration via the NLRP3 inflammasome (Figure 4D). Iron toxicity in the retina and other tissues is widely attributed to catalysis of hydroxyl radicals via Fenton's reaction. However, our findings reveal that, absent SINE RNA accumulation or caspase-1 signaling, iron overload is not sufficient to drive degeneration of the retina. We further report that iron-overload-induced *Alu* RNA/inflammasome-mediated retinal toxicity is not a generic response to excess of Fenton catalysts, as this pathway was not common to chromium-, copper-, or zinc-induced retinal toxicity.

Although our data suggest that hydroxyl radical formation is not sufficient to drive inflammasome-mediated retinal toxicity, the necessity of iron-mediated hydroxyl radical formation on *Alu* RNA-mediated iron toxicity is not known. We previously reported that *Alu* RNAs induce mitochondrial reactive oxygen species generation, which is an essential component of its inflammasome signaling and toxicity (Tarallo et al., 2012). That *Alu* RNA signaling involves reactive oxygen species generation and iron's ability to catalyze free radical formation suggests that Fenton activity of iron could augment *Alu* RNA toxicity.

Iron antagonism of DICER1 in the RPE likely impacts not only *Alu* RNA metabolism but microRNA biogenesis as well. Although we previously found no anatomical disruption of microRNA-deficient RPE of adult mice (RPE-specific knockouts of Drosha, Dgcr8, and argonaute-2 appeared normal upon fundus and flat mount examination; Tarallo et al., 2012), we cannot exclude the possibility that global microRNA perturbation due to DICER1 inhibition also contributes to or modulates iron-overload-induced retinal toxicity.

These findings also provide support for pathogenic roles for both inflammasome activation and iron overload in human AMD. Inflammasome signaling in human AMD tissues has now been observed by multiple laboratories (Chan et al., 2013; Tarallo et al., 2012; Tseng et al., 2013). Experimentally, multiple AMD-related stimuli including *Alu* RNA (Kerur et al., 2013; Tseng et al., 2013), A2E (Anderson et al., 2013), complement cascade components (Doyle et al., 2012; Triantafilou et al., 2013), amyloid-β (Liu et al., 2013), and excess VEGF-A (Marneros, 2013) have been reported to act via inflammasome signaling. Our results suggest that targeting inflammasome signaling components as a "next-generation" therapeutic for AMD may provide additional, unanticipated benefits with respect to phenotypes arising from iron overload. Notably, our findings reveal that

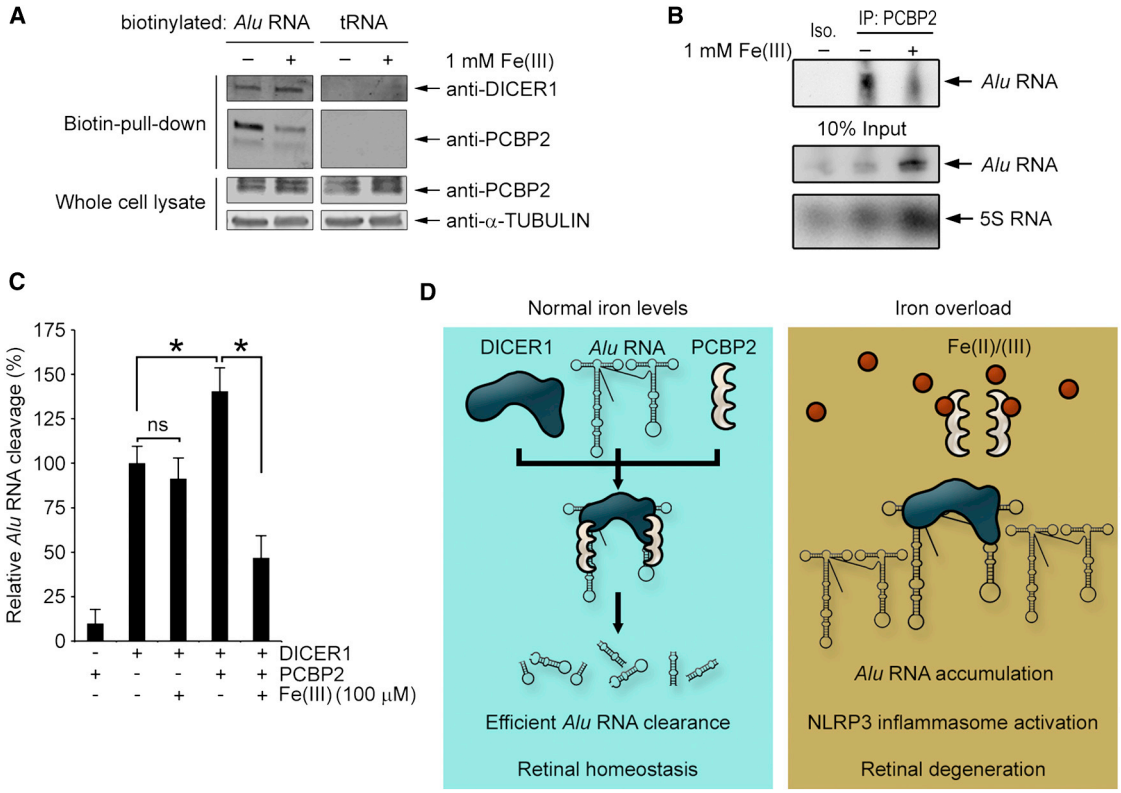

Figure 4. Iron Sensitivity of DICER1 Processing of *Alu* RNAs Is Mediated by PCBP2

(A) Western blotting of streptavidin-mediated pull-down and whole-cell lysates from biotin-*Alu* or biotin-tRNA-transfected human ARPE-19 cells that were exposed to 1 mM Fe(III).

(B) Northern blotting of native *Alu* and 5S RNAs in human ARPE-19 exposed to 1 mM Fe(III) following immuno-precipitation with anti-PCBP2 antibody or in whole-cell lysates.

(C) DICER1-mediated *Alu* RNA cleavage quantified from in vitro dicing reactions containing recombinant human DICER1, recombinant human PCBP2, and 100 μM Fe(III) where indicated. For all panels, n = 3–6; *p < 0.05. Error bars denote SEM.

(D) Proposed model of iron-overload-induced retinal toxicity, involving the sequestration of PCBP2 from *Alu* RNA/DICER1 complexes, leading to an accumulation of *Alu* RNAs, NLRP3 inflammasome activation, and retinal degeneration.

NLRP3 alone does not account for the entirety of iron-induced RPE degeneration. Therefore, it will be important in future studies to determine the extent to which NLRP3-independent inflammasome activation contributes to the AMD and pathological effects of AMD-related inflammasome agonists. Further, our studies utilized a mouse line lacking both caspase-1 and the non-canonical inflammasome component caspase-11, which were protected from treatment with a relatively high dose of iron. Whether non-canonical inflammasome activation is required for iron-induced toxicity is an important future direction for study.

PCBP2 is an RNA-binding protein and iron chaperone, with diverse cellular functions such as RNA stability (Czyzyk-Krzeska and Bendixen, 1999; Paulding and Czyzyk-Krzeska, 1999; Xin et al., 2011), protein stability (You et al., 2009), immunity (Blyn et al., 1996, 1997; You et al., 2009), microRNA processing (Li et al., 2012), iron homeostasis (Lane and Richardson, 2014), preventing stress-induced apoptosis (Ghosh et al., 2008), cell growth (Han et al., 2013; Waggoner et al., 2009), and tumor growth (Han et al., 2013; Hu et al., 2014). The extent to which these diverse functions of PCBP2, as well as its SINE RNA-processing activity, contribute to inflammasome activation and iron-induced RPE degeneration in geographic atrophy warrants further investigation.

Iron overload has been observed in numerous neurodegenerative disorders including in senile plaques and neurofibrillary tangles of human cadaver brains with Alzheimer's disease (Quintana et al., 2006; Sayre et al., 2000; Smith et al., 1997) and in the substantia nigra of humans with Parkinson's disease (Ayton and Lei, 2014; Dexter et al., 1987). Interestingly, the involvement of the NLRP3 inflammasome has been independently implicated in the pathogenesis of these diseases (Codolo et al., 2013; Freeman et al., 2013; Heneka et al., 2013). This study raises the intriguing possibility that the damaging effects of *Alu* RNA accretion due to iron overload could extend beyond AMD and contribute to neurodegenerative diseases with recognized etiological similarities. These findings also raise the interesting possibility that systemic iron overload promotes NLRP3 inflammasome activation outside of the eye, such as in hepatic macrophages, where inflammatory phenotypes such as NF-κB activation and cytokine expression are noted effects of iron overload in liver injury (Lin et al., 1997; Xiong et al., 2008).

EXPERIMENTAL PROCEDURES

Intraocular Injections and Imaging

All animal experiments were in accordance with the guidelines of the University of Kentucky Institutional Animal Care and Use Committee and the Association for Research in Vision and Ophthalmology. Subretinal injections and intravitreous injections (1 μl each) were performed with a 35-gauge Exmire microsyringe (Ito). Fundus imaging was performed on a TRC-50 IX camera (Topcon) linked to a digital imaging system (Sony). RPE flat mounts were immunolabeled using antibodies against Zonula Occludens-1 (Invitrogen) and visualized by confocal microscopy (Leica Microsystems). Cryosections of 4% PFA fixed retinal cross-sections were immuno-labeled with anti-Nlrp3 (Abcam) and visualized by fluorescent microscopy (Nikon).

RNA and Protein Abundance Analysis

In situ hybridization was performed on frozen, fixed tissue sections from Ceph$^{-/-}$/Heph$^{-/-}$, and wild-type (C57BL/6J) age-matched mice were processed using custom designed probes for B1 and B2 RNAs (Advanced Cell Diagnostics) according to the manufacturer's instructions. Probes were visualized by confocal microscopy (Leica Microsystems). Quantities of B1, B2 U6, and 5S RNAs were determined by northern blotting. Protein abundance was measured by western blotting with the following primary antibodies: mouse-anti-PCBP2 (Abnova; 1:500), rabbit-anti-DICER1 (Bethyl Laboratories; 1:1,000), mouse-anti-α-tubulin (Sigma; 1:1,000), rabbit-anti-caspase-1 (Invitrogen, 1:1,000 or Abcam, 1:1,000), mouse-anti-NLRP3 (Enzo Life Sciences; 1:1,000), anti-β-actin (Sigma-Aldrich; 1:1,000), and rabbit-anti-vinculin (Sigma-Aldrich; 1:1,000).

Statistical Analysis

Results are expressed as mean ± SEM, with p values < 0.05 considered statistically significant. Differences between groups were compared by Mann-Whitney U test or Student's t test, as appropriate.

SUPPLEMENTAL INFORMATION

Supplemental Information includes Supplemental Experimental Procedures and three figures and can be found with this article online at http://dx.doi.org/10.1016/j.celrep.2015.05.023.

AUTHOR CONTRIBUTIONS

B.D.G., C.B.W., Y.K., T.Y., R.Y., S.L., B.J.F., A.B.-C., N.K., A.U., Y.S.H., D.L., M.E.K., and W.H.M. performed experiments. G.N., P.G., and J.L.D. provided reagents. B.D.G. conceived and directed the project and wrote the paper with assistance from J.A. All authors had the opportunity to discuss the results and comment on the manuscript.

ACKNOWLEDGMENTS

Vector to express recombinant human PCBP2 was provided by Dr. Peng Jin (Emory University). L. Toll, G.R. Pattison, R. King, L. Xu, M. McConnell, C. Payne, D. Robertson, and G. Botzet provided technical assistance. B.D.G. was supported by American Heart Association and International Retinal Research Foundation (IRRF); T.Y. was supported by Fight for Sight postdoctoral award; J.A. was supported by NIH grants (DP1GM114862, R01EY018350, R01EY018836, R01EY020672, R01EY022238, and R01EY024068), Doris Duke Distinguished Clinical Scientist Award, Burroughs Wellcome Fund Clinical Scientist Award in Translational Research, Ellison Medical Foundation Senior Scholar in Aging Award, Foundation Fighting Blindness Individual Investigator Research Award, Harrington Discovery Institute Scholar-Innovator Award, Dr. E. Vernon Smith and Eloise C. Smith Macular Degeneration Endowed Chair, and Research to Prevent Blindness departmental unrestricted grant; B.J.F. was supported by NIH T32HL091812 and UL1RR033173; A.B.-C. was supported by the Programme for Advanced Medical Education (sponsored by Fundação Calouste Gulbenkian, Fundação Champalimaud, Ministério da Saúde, and Fundação para a Ciência e Tecnologia, Portugal) and Bayer Global Ophthalmology Research Award; Y.K. was supported by Alcon Japan Research award; N.K. was supported by Beckman Initiative for Macular Research and NIH K99EY024336; and C.B.W. was supported by The Loris and David Rich Postdoctoral Scholar Award (IRRF). J.A. and B.J.F. are named as inventors on patent applications relating to the treatment of macular degeneration filed by their employer, the University of Kentucky. J.A. is a co-founder of iVeena (Holdings, Pharma, Delivery), which has licensed some of this technology from the University of Kentucky. J.A. has received honoraria from Allergan.

Received: December 11, 2014
Revised: March 23, 2015
Accepted: May 8, 2015
Published: June 11, 2015

REFERENCES

Anderson, O.A., Finkelstein, A., and Shima, D.T. (2013). A2E induces IL-1ß production in retinal pigment epithelial cells via the NLRP3 inflammasome. PLoS ONE *8*, e67263.

Ayton, S., and Lei, P. (2014). Nigral iron elevation is an invariable feature of Parkinson's disease and is a sufficient cause of neurodegeneration. BioMed Res. Int. *2014*, 581256.

Blyn, L.B., Swiderek, K.M., Richards, O., Stahl, D.C., Semler, B.L., and Ehrenfeld, E. (1996). Poly(rC) binding protein 2 binds to stem-loop IV of the poliovirus RNA 5′ noncoding region: identification by automated liquid chromatography-tandem mass spectrometry. Proc. Natl. Acad. Sci. USA *93*, 11115–11120.

Blyn, L.B., Towner, J.S., Semler, B.L., and Ehrenfeld, E. (1997). Requirement of poly(rC) binding protein 2 for translation of poliovirus RNA. J. Virol. *71*, 6243–6246.

Chan, C., Shen, D., Wang, Y., Chu, X., Abu-Asab, M., and Tuo, J. (2013). Inflammasomes in human eyes with AMD and mouse retinas with focal retinal degeneration (Seattle, WA: ARVO Annual Meeting). http://www.arvo.org/webs/am2013/abstract/section/retinal_cell_biology.pdf.

Codolo, G., Plotegher, N., Pozzobon, T., Brucale, M., Tessari, I., Bubacco, L., and de Bernard, M. (2013). Triggering of inflammasome by aggregated α-synuclein, an inflammatory response in synucleinopathies. PLoS ONE *8*, e55375.

Czyzyk-Krzeska, M.F., and Bendixen, A.C. (1999). Identification of the poly(C) binding protein in the complex associated with the 3′ untranslated region of erythropoietin messenger RNA. Blood *93*, 2111–2120.

Dexter, D.T., Wells, F.R., Agid, F., Agid, Y., Lees, A.J., Jenner, P., and Marsden, C.D. (1987). Increased nigral iron content in postmortem parkinsonian brain. Lancet *2*, 1219–1220.

Doyle, S.L., Campbell, M., Ozaki, E., Salomon, R.G., Mori, A., Kenna, P.F., Farrar, G.J., Kiang, A.S., Humphries, M.M., Lavelle, E.C., et al. (2012). NLRP3 has a protective role in age-related macular degeneration through the induction of IL-18 by drusen components. Nat. Med. *18*, 791–798.

Dridi, S., Hirano, Y., Tarallo, V., Kim, Y., Fowler, B.J., Ambati, B.K., Bogdanovich, S., Chiodo, V.A., Hauswirth, W.W., Kugel, J.F., et al. (2012). ERK1/2 activation is a therapeutic target in age-related macular degeneration. Proc. Natl. Acad. Sci. USA *109*, 13781–13786.

Flinn, J.M., Kakalec, P., Tappero, R., Jones, B., and Lengyel, I. (2014). Correlations in distribution and concentration of calcium, copper and iron with zinc in isolated extracellular deposits associated with age-related macular degeneration. Metallomics *6*, 1223–1228.

Fowler, B.J., Gelfand, B.D., Kim, Y., Kerur, N., Tarallo, V., Hirano, Y., Amarnath, S., Fowler, D.H., Radwan, M., Young, M.T., et al. (2014). Nucleoside reverse transcriptase inhibitors possess intrinsic anti-inflammatory activity. Science *346*, 1000–1003.

Freeman, D., Cedillos, R., Choyke, S., Lukic, Z., McGuire, K., Marvin, S., Burrage, A.M., Sudholt, S., Rana, A., O'Connor, C., et al. (2013). Alpha-synuclein induces lysosomal rupture and cathepsin dependent reactive oxygen species following endocytosis. PLoS ONE *8*, e62143.

Ghosh, D., Srivastava, G.P., Xu, D., Schulz, L.C., and Roberts, R.M. (2008). A link between SIN1 (MAPKAP1) and poly(rC) binding protein 2 (PCBP2) in counteracting environmental stress. Proc. Natl. Acad. Sci. USA *105*, 11673–11678.

Gnana-Prakasam, J.P., Tawfik, A., Romej, M., Ananth, S., Martin, P.M., Smith, S.B., and Ganapathy, V. (2012). Iron-mediated retinal degeneration in haemojuvelin-knockout mice. Biochem. J. *441*, 599–608.

Hadziahmetovic, M., Dentchev, T., Song, Y., Haddad, N., He, X., Hahn, P., Pratico, D., Wen, R., Harris, Z.L., Lambris, J.D., et al. (2008). Ceruloplasmin/hephaestin knockout mice model morphologic and molecular features of AMD. Invest. Ophthalmol. Vis. Sci. *49*, 2728–2736.

Hahn, P., Milam, A.H., and Dunaief, J.L. (2003). Maculas affected by age-related macular degeneration contain increased chelatable iron in the retinal pigment epithelium and Bruch's membrane. Arch. Ophthalmol. *121*, 1099–1105.

Hahn, P., Qian, Y., Dentchev, T., Chen, L., Beard, J., Harris, Z.L., and Dunaief, J.L. (2004). Disruption of ceruloplasmin and hephaestin in mice causes retinal iron overload and retinal degeneration with features of age-related macular degeneration. Proc. Natl. Acad. Sci. USA *101*, 13850–13855.

Han, W., Xin, Z., Zhao, Z., Bao, W., Lin, X., Yin, B., Zhao, J., Yuan, J., Qiang, B., and Peng, X. (2013). RNA-binding protein PCBP2 modulates glioma growth by regulating FHL3. J. Clin. Invest. *123*, 2103–2118.

Heneka, M.T., Kummer, M.P., Stutz, A., Delekate, A., Schwartz, S., Vieira-Saecker, A., Griep, A., Axt, D., Remus, A., Tzeng, T.C., et al. (2013). NLRP3 is activated in Alzheimer's disease and contributes to pathology in APP/PS1 mice. Nature *493*, 674–678.

Hu, Q., Tanasa, B., Trabucchi, M., Li, W., Zhang, J., Ohgi, K.A., Rose, D.W., Glass, C.K., and Rosenfeld, M.G. (2012). DICER- and AGO3-dependent generation of retinoic acid-induced DR2 Alu RNAs regulates human stem cell proliferation. Nat. Struct. Mol. Biol. *19*, 1168–1175.

Hu, C.E., Liu, Y.C., Zhang, H.D., and Huang, G.J. (2014). The RNA-binding protein PCBP2 facilitates gastric carcinoma growth by targeting miR-34a. Biochem. Biophys. Res. Commun. *448*, 437–442.

Jünemann, A.G., Stopa, P., Michalke, B., Chaudhri, A., Reulbach, U., Huchzermeyer, C., Schlötzer-Schrehardt, U., Kruse, F.E., Zrenner, E., and Rejdak, R. (2013). Levels of aqueous humor trace elements in patients with non-exsudative age-related macular degeneration: a case-control study. PLoS ONE *8*, e56734.

Jurka, J., Kohany, O., Pavlicek, A., Kapitonov, V.V., and Jurka, M.V. (2005). Clustering, duplication and chromosomal distribution of mouse SINE retrotransposons. Cytogenet. Genome Res. *110*, 117–123.

Kaneko, H., Dridi, S., Tarallo, V., Gelfand, B.D., Fowler, B.J., Cho, W.G., Kleinman, M.E., Ponicsan, S.L., Hauswirth, W.W., Chiodo, V.A., et al. (2011). DICER1 deficit induces Alu RNA toxicity in age-related macular degeneration. Nature *471*, 325–330.

Kauppinen, A., Niskanen, H., Suuronen, T., Kinnunen, K., Salminen, A., and Kaarniranta, K. (2012). Oxidative stress activates NLRP3 inflammasomes in ARPE-19 cells—implications for age-related macular degeneration (AMD). Immunol. Lett. *147*, 29–33.

Kerur, N., Hirano, Y., Tarallo, V., Fowler, B.J., Bastos-Carvalho, A., Yasuma, T., Yasuma, R., Kim, Y., Hinton, D.R., Kirschning, C.J., et al. (2013). TLR-independent and P2X7-dependent signaling mediate Alu RNA-induced NLRP3 inflammasome activation in geographic atrophy. Invest. Ophthalmol. Vis. Sci. *54*, 7395–7401.

Lane, D.J., and Richardson, D.R. (2014). Chaperone turns gatekeeper: PCBP2 and DMT1 form an iron-transport pipeline. Biochem. J. *462*, e1–e3.

Li, Y., Lin, L., Li, Z., Ye, X., Xiong, K., Aryal, B., Xu, Z., Paroo, Z., Liu, Q., He, C., and Jin, P. (2012). Iron homeostasis regulates the activity of the microRNA pathway through poly(C)-binding protein 2. Cell Metab. *15*, 895–904.

Lin, M., Rippe, R.A., Niemelä, O., Brittenham, G., and Tsukamoto, H. (1997). Role of iron in NF-kappa B activation and cytokine gene expression by rat hepatic macrophages. Am. J. Physiol. *272*, G1355–G1364.

Liu, R.T., Gao, J., Cao, S., Sandhu, N., Cui, J.Z., Chou, C.L., Fang, E., and Matsubara, J.A. (2013). Inflammatory mediators induced by amyloid-beta in the retina and RPE in vivo: implications for inflammasome activation in age-related macular degeneration. Invest. Ophthalmol. Vis. Sci. *54*, 2225–2237.

Marneros, A.G. (2013). NLRP3 inflammasome blockade inhibits VEGF-A-induced age-related macular degeneration. Cell Rep. *4*, 945–958.

Mori, M.A., Raghavan, P., Thomou, T., Boucher, J., Robida-Stubbs, S., Macotela, Y., Russell, S.J., Kirkland, J.L., Blackwell, T.K., and Kahn, C.R. (2012). Role of microRNA processing in adipose tissue in stress defense and longevity. Cell Metab. *16*, 336–347.

Paulding, W.R., and Czyzyk-Krzeska, M.F. (1999). Regulation of tyrosine hydroxylase mRNA stability by protein-binding, pyrimidine-rich sequence in the 3′-untranslated region. J. Biol. Chem. *274*, 2532–2538.

Quintana, C., Bellefqih, S., Laval, J.Y., Guerquin-Kern, J.L., Wu, T.D., Avila, J., Ferrer, I., Arranz, R., and Patiño, C. (2006). Study of the localization of iron, ferritin, and hemosiderin in Alzheimer's disease hippocampus by analytical microscopy at the subcellular level. J. Struct. Biol. *153*, 42–54.

Ren, Y.F., Li, G., Wu, J., Xue, Y.F., Song, Y.J., Lv, L., Zhang, X.J., and Tang, K.F. (2012). Dicer-dependent biogenesis of small RNAs derived from 7SL RNA. PLoS ONE *7*, e40705.

Ren, Y.F., Li, G., Xue, Y.F., Zhang, X.J., Song, Y.J., Lv, L., Wu, J., Fang, Y.X., Wang, Y.Q., Shi, K.Q., et al. (2013). Decreased dicer expression enhances SRP-mediated protein targeting. PLoS ONE *8*, e56950.

Sayre, L.M., Perry, G., Harris, P.L., Liu, Y., Schubert, K.A., and Smith, M.A. (2000). In situ oxidative catalysis by neurofibrillary tangles and senile plaques in Alzheimer's disease: a central role for bound transition metals. J. Neurochem. *74*, 270–279.

Smith, M.A., Harris, P.L., Sayre, L.M., and Perry, G. (1997). Iron accumulation in Alzheimer disease is a source of redox-generated free radicals. Proc. Natl. Acad. Sci. USA *94*, 9866–9868.

Tarallo, V., Hirano, Y., Gelfand, B.D., Dridi, S., Kerur, N., Kim, Y., Cho, W.G., Kaneko, H., Fowler, B.J., Bogdanovich, S., et al. (2012). DICER1 loss and Alu RNA induce age-related macular degeneration via the NLRP3 inflammasome and MyD88. Cell *149*, 847–859.

Triantafilou, K., Hughes, T.R., Triantafilou, M., and Morgan, B.P. (2013). The complement membrane attack complex triggers intracellular Ca2+ fluxes leading to NLRP3 inflammasome activation. J. Cell Sci. *126*, 2903–2913.

Tseng, W.A., Thein, T., Kinnunen, K., Lashkari, K., Gregory, M.S., D'Amore, P.A., and Ksander, B.R. (2013). NLRP3 inflammasome activation in retinal pigment epithelial cells by lysosomal destabilization: implications for age-related macular degeneration. Invest. Ophthalmol. Vis. Sci. *54*, 110–120.

Urrutia, P.J., Mena, N.P., and Núñez, M.T. (2014). The interplay between iron accumulation, mitochondrial dysfunction, and inflammation during the execution step of neurodegenerative disorders. Front. Pharmacol. *5*, 38.

Waggoner, S.A., Johannes, G.J., and Liebhaber, S.A. (2009). Depletion of the poly(C)-binding proteins alphaCP1 and alphaCP2 from K562 cells leads to p53-independent induction of cyclin-dependent kinase inhibitor (CDKN1A) and G1 arrest. J. Biol. Chem. *284*, 9039–9049.

Wiesen, J.L., and Tomasi, T.B. (2009). Dicer is regulated by cellular stresses and interferons. Mol. Immunol. *46*, 1222–1228.

Xin, Z., Han, W., Zhao, Z., Xia, Q., Yin, B., Yuan, J., and Peng, X. (2011). PCBP2 enhances the antiviral activity of IFN-α against HCV by stabilizing the mRNA of STAT1 and STAT2. PLoS ONE *6*, e25419.

Xiong, S., She, H., Zhang, A.S., Wang, J., Mkrtchyan, H., Dynnyk, A., Gordeuk, V.R., French, S.W., Enns, C.A., and Tsukamoto, H. (2008). Hepatic macrophage iron aggravates experimental alcoholic steatohepatitis. Am. J. Physiol. Gastrointest. Liver Physiol. *295*, G512–G521.

Yan, Y., Salazar, T.E., Dominguez, J.M., 2nd, Nguyen, D.V., Li Calzi, S., Bhatwadekar, A.D., Qi, X., Busik, J.V., Boulton, M.E., and Grant, M.B. (2013). Dicer expression exhibits a tissue-specific diurnal pattern that is lost during aging and in diabetes. PLoS ONE *8*, e80029.

You, F., Sun, H., Zhou, X., Sun, W., Liang, S., Zhai, Z., and Jiang, Z. (2009). PCBP2 mediates degradation of the adaptor MAVS via the HECT ubiquitin ligase AIP4. Nat. Immunol. *10*, 1300–1308.